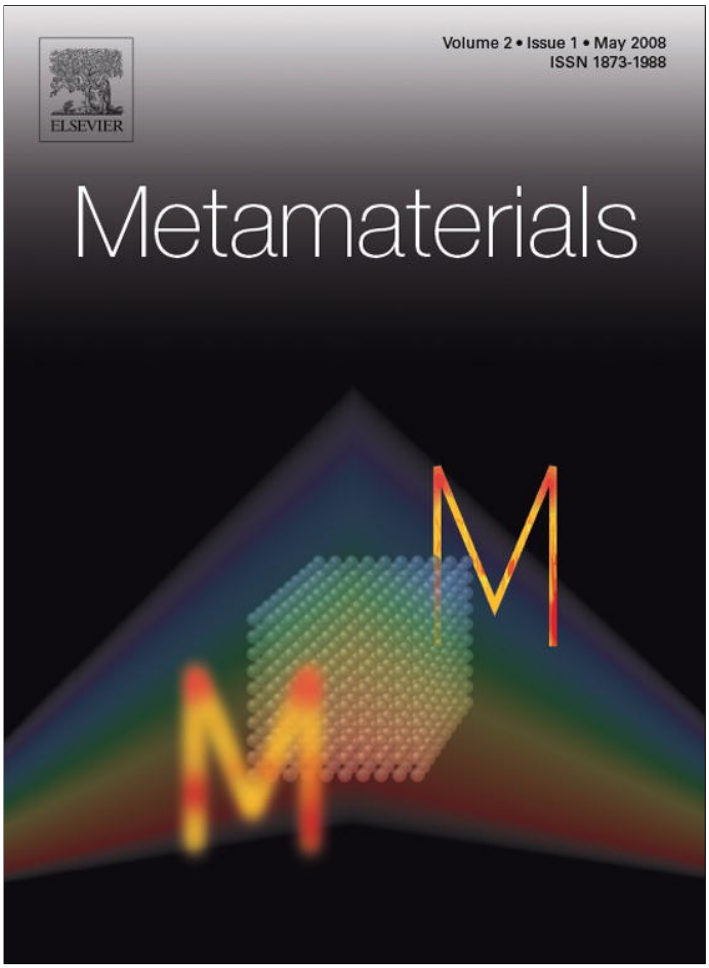

Available online at www.sciencedirect.com
ScienceDirect
Metamaterials 2 (2008) 45–51
Metamaterials
www.elsevier.com/locate/metmat

# Plasmonic nanoantenna arrays for the visible

Zhengtong Liu [a], Alexandra Boltasseva [b], Rasmus H. Pedersen [c], Reuben Bakker [a], Alexander V. Kildishev [a], Vladimir P. Drachev [a], Vladimir M. Shalaev [a,*]

[a] *School of Electrical and Computer Engineering and Birck Nanotechnology Center, Purdue University, West Lafayette, IN 47907, USA*
[b] *DTU Fotonik, Department of Photonics Engineering, Technical University of Denmark, DK-2800 Kgs Lyngby, Denmark*
[c] *DTU Nanotech, Department of Micro and Nanotechnology, Technical University of Denmark, DK-2800 Kgs Lyngby, Denmark*

Received 20 December 2007; received in revised form 4 March 2008; accepted 10 March 2008
Available online 14 March 2008

**Abstract**

Gold nanoantenna arrays composed of paired elliptical cylinders are fabricated and studied experimentally and numerically. The arrays show far-field spectra resonances in the visible range for two orthogonal polarizations. Finite element method is used to accurately simulate the far-field spectra with modified gold optical properties. The resonance wavelengths and electrical field enhancement are studied as functions of the antenna dimensions. The field enhancement is found to be inversely proportional to the gap size.


*Keywords:* Drude–Lorentz model; Near-field optics; Plasmonics

Optical nanoantennas have been of great interest recently due to their ability to support a highly efficient, localized surface plasmon resonance and produce significantly enhanced and highly confined electromagnetic fields. Such enhanced local fields have many applications such as biosensors, near-field scanning optical microscopy (NSOM), quantum optical information processing, enhanced Raman scattering as well as other optical processes [1–9]. A nanoantenna mounted on a NSOM tip can achieve sub-diffraction resolution and modify the fluorescent properties of light emitters in the vicinity of the nanoantenna [10–12]. A optical nanoantenna embedded on the facet of a diode laser is capable of generating enhanced and spatially confined optical near fields, which can be used in optical storage and NSOM [13]. Nanoantennas are also used in nanometer-scale optical lithography [14]. In most of the studies, the optical nanoantennas consist of paired metallic nanostructures including 2D structures such as metal strips [2,15–17] and 3D structures such as nanorods [1,12,18], bow-tie particles [10,11,19–24], nanodiscs [25,26], spheres [27], and other shapes like core-shell structures [28–30]. It has been shown theoretically and experimentally that such structures can produce strong resonance and large field enhancement.

The electrodynamics of optical nanoantennas have been simulated by several groups using Green's tensor technique [1], the finite element method (FEM) [2], finite difference time domain (FDTD) methods [14,19,20,24], the Fourier modal method [25], discrete dipole approximations (DDA) [22,26,28], and the boundary element method [18,28]. Although some simulation results were compared to experimental results [19,24], there is still a

* Corresponding author. Tel.: +1 765 494 9855; fax: +1 765 496 6443.
*E-mail address:* shalaev@purdue.edu (V.M. Shalaev).

1873-1988/$ – see front matter © 2008 Elsevier B.V. All rights reserved.
doi:10.1016/j.metmat.2008.03.001

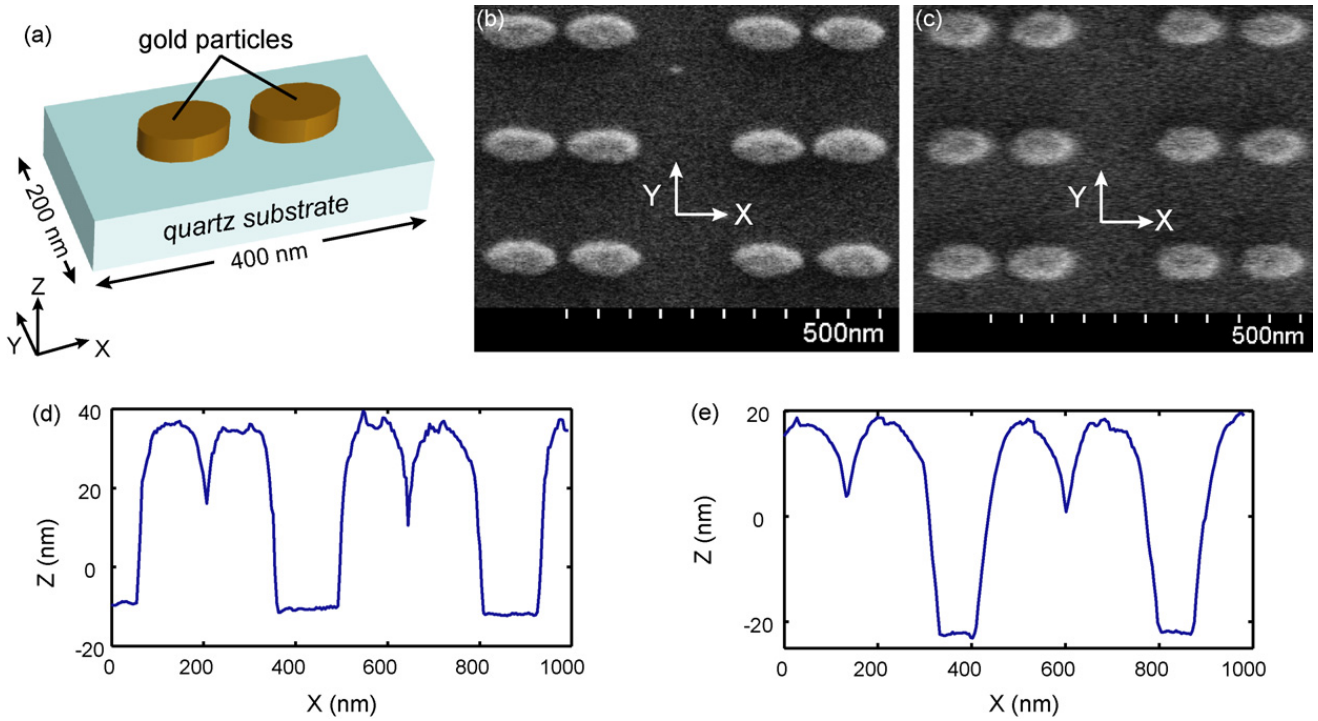


Fig. 1. (a) The schematic of a unit cell; (b and c) FESEM images of the samples A and B; (d and e) surface profiles measured by AFM of samples A and B.

lack of direct matching between theoretical and experimental results in the visible range that can verify the validity of the simulation methods. In this report we use FEM to simulate experimentally measured far-field optical transmittance and reflectance spectra of nanoantenna arrays. We show that with modified material properties taken into account, excellent matching can be achieved between experimental and simulated data. The FEM model is also used to study the resonance–geometry relationship and the optical near-field distribution. The near-field maps obtained by FEM modeling are compared with NSOM measurements elsewhere [31].

## 1. Experimental details

Two samples of paired gold nanoantenna arrays, named A and B, were designed and fabricated. The arrays are composed of gold nanoparticles with elliptic cylinder shapes. Each unit cell has two nanoparticles with a gap between the two particles along their major axes (Fig. 1(a)). The periods along the major and minor axes are 400 and 200 nm, respectively. The fabrication process is as follows: a quartz substrate is first spin-coated with the positive e-beam resist ZEP520A, and a 20-nm-thick film of aluminum is deposited by thermal evaporation on top of the resist to act as a charge-distribution layer during electron beam lithography (EBL). The nanoantenna array pattern is defined by 100 kV EBL (JEOL JBX-9300FS). The aluminum layer is removed in Microposit® MF-322 and the pattern developed in ZED-N50. A layer of gold 40 nm thick is then deposited by e-beam evaporation, and a lift-off process in Microposit® remover 1165 completes the procedure. The size of the arrays is 150 μm × 150 μm.

The samples were then examined by field emission electron scanning microscopy (FESEM) and atomic force microscopy (AFM). Representative FESEM images and AFM profiles are shown in Fig. 1(b–e). Although all unit cells in an array have the same design, each particle randomly deviates from the designed shape to certain extent. In sample A the major axis ranges from 104 to 118 nm, the minor axis from 52 to 62 nm, and the gap from 12 to 27 nm. In sample B the major axis ranges from 105 to 117 nm, the minor axis from 54 to 65 nm, and the gap from 22 to 37 nm. We observe from the FESEM images that both samples are very similar except for the gap sizes: sample A has a gap approximately 10 nm smaller than B. The AFM images show that the surface roughness of the gold nanoparticles is around 1 nm.

The transmittance and reflectance spectra of these samples were measured in the visible range with incident light normal to the sample surface. The incident light was linearly polarized, and we used two polarizations: the principal polarization where the electric field is parallel to the major axis and the secondary polariza-

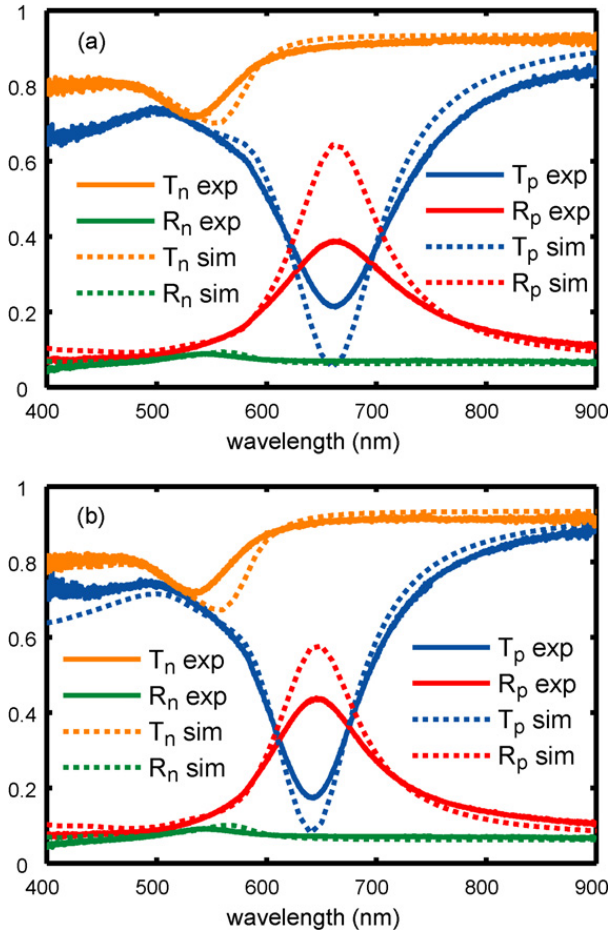


Fig. 2. The experimental (exp) and simulated (sim) transmittance ($T$) and reflectance ($R$) spectra for both principal (p) and secondary (n) polarization of sample A (a) and sample B (b).

tion where the electric field is normal to the major axis. The measured spectra are shown in Fig. 2. Both samples show strong resonances for the principal polarization, one at 660 nm and the other at 640 nm. Since the only significant difference between the two samples is that the gap of sample A gap is roughly 10 nm smaller than that of sample B, we conclude that the change of gap size shifts the resonance. This is confirmed by numerical simulation results. For the secondary polarization only a weak resonance is visible, and both samples have virtually identical spectra, which indicates that the gap does not affect this resonance.

## 2. Simulation results and discussion

A FEM model was created using a commercial package (COMSOL Multiphysics) to simulate the electrodynamics of the nanoantenna arrays. The dielectric constants of gold were obtained from literature [32]. The dimensions of the major axis, the minor axis, and the gap in the FEM models were tuned in order to match the simulated resonance wavelengths to the experimental results, and the resulting dimensions used in simulations are as follows: for sample A, the major axis is 110 nm, minor axis 55 nm, and gap 17 nm; for sample B the major axis is 108 nm, minor axis 58 nm, and gap 28 nm. These values are all within the range of dimensions obtained from SEM measurements. The 40 nm thickness and the 400 and 200 nm periods along the major axis and minor axis, respectively, were taken from the initial design. The results are compared with the experimental spectra in Fig. 2.

Although the resonance wavelengths for the principal polarization obtained from simulations match those from experiments, the shapes of the spectra are very different. Varying the dimensions in the simulations of the nanoantenna arrays cannot further reduce the differences. Possible reasons for this discrepancy are the size effect and the surface roughness, which may affect gold optical properties and particle coupling [33–36]. Since both effects may result in a broadening of the absorption band, one can model this combined effect by modifying the gold optical constants [37–39]. As a first step, the Drude–Lorentz model (DLM)

$$\varepsilon = 1 - \frac{\omega_p^2}{\omega^2 + i\Gamma_p\omega} + \sum_m \frac{f_m\omega_m^2}{\omega_m^2 - \omega^2 - i\Gamma_m\omega} \qquad (1)$$

is used to fit the experimental optical constants of gold from the literature [32]. Here $\omega_p$ is the plasmon frequency, $\Gamma_p$ is the damping constant, and $\omega_m$ and $\Gamma_m$ are the resonant frequency and the damping constants of the $m$th Lorentz oscillator, respectively. The Drude–Lorentz model has two terms: the Drude term and the sum of Lorentz terms. The Drude term describes the free electron response and is widely used to characterize the optical properties of metals at relatively low frequencies. The sum of the Lorentz terms gives the contribution from Lorentzian oscillators due to interband transitions, which is common for dielectric materials and for metals at high frequencies. In the fitting, three Lorentzian oscillators together with the Drude term (with the known parameters [32] $\omega_p = 9$ eV and $\Gamma_p = 0.07$ eV) are used to describe the gold dielectric constants above wavelengths of 400 nm; the fitting parameters are $\omega_1 = 2.7$ eV, $f_1 = 0.4$, $\Gamma_1 = 0.4$ eV, $\omega_2 = 3.1$ eV, $f_2 = 0.9$, $\Gamma_2 = 0.6$ eV, $\omega_3 = 15$ eV, $f_3 = 6.1$, and $\Gamma_3 = 1.6$ eV. The surface roughness effect as well as possible size effect on the optical spectra in fabricated nanostructures can then be modeled by modifying the damping constant $\Gamma_p$ in bulk metal. We introduce a loss factor $\alpha$ to represent this change so the modified Drude term damping constant is $\alpha\Gamma_p$. The real and imaginary parts of the permittivity of gold with $\alpha = 2$

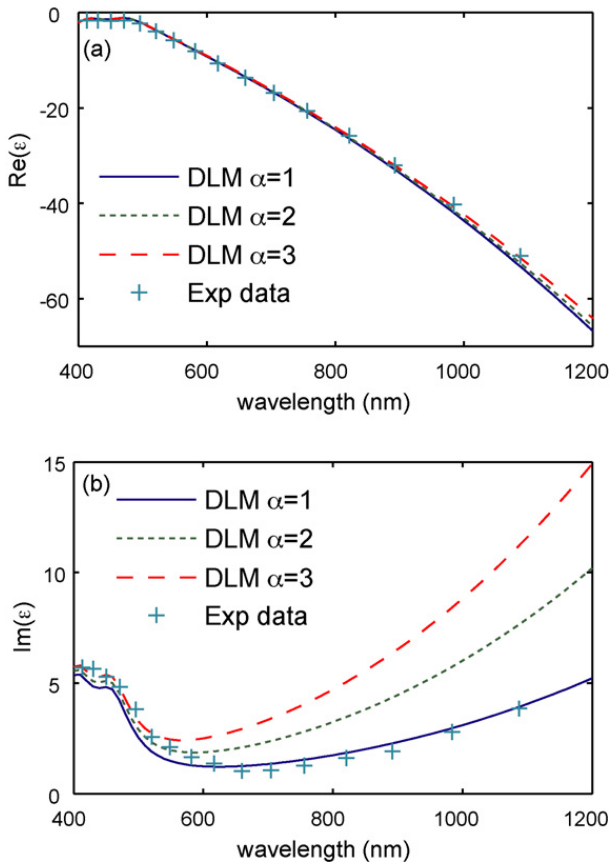


Fig. 3. The real (a) and imaginary (b) parts of permittivity of bulk Au: the experimental data (from literature [32]), the fitted curves with the Drude–Lorentz model (DLM $\alpha = 1$), and calculated curves with loss factor $\alpha = 2$ and $\alpha = 3$.

and $\alpha = 3$ are shown in Fig. 3. The change to $\Gamma_p$ of bulk gold modifies the imaginary part of the permittivity in the long wavelength range significantly, but it has only a slight effect at shorter wavelengths. The real part of the permittivity is essentially unchanged in the frequency range of interest.

We applied the modified gold optical constants to the FEM model to simulate the spectra for the nanoantenna array. The results are plotted in Fig. 4 together with the experimental results for comparison. Although the variation of $\alpha$ does not shift the resonance wavelengths, it does change resonance strength for the principal polarization and improves the agreement between simulation and experimental results. For sample A the simulated spectra with $\alpha = 3$ match the experimental spectra almost perfectly, while for sample B $\alpha = 2$ gives the best fit. The reason that samples A and B need different loss factors to fit the experimental spectra is likely due to the fact that sample A has a smaller gap and hence higher field strength inside the gap, therefore the surface roughness effects is stronger than in sample B. For the secondary polarization, the different loss factors have smaller effects on the spectra because the resonance wavelength is very close to the interband transition wavelength, so the change in the Drude term does not affect the optical properties near the resonance drastically.

With the addition of the loss factor, the simulations match the experiments well, which provides confidence in the FEM model. We then used this same model to study the nanoantenna's geometry–resonance relationship. Since the change of $\alpha$ does not shift the resonance, for simplicity we assume $\alpha = 3$ in the remainder of this paper. The major axis, minor axis, and gap in sample A were individually varied while other dimensions were kept the same as in the actual device. The corresponding resonant wavelengths were plotted versus the dimensions (Fig. 5). All these dimensions affect resonance in different ways. Increasing the major axis red-shifts the resonance almost linearly, and the linear dependence on the major axis is similar to a thin, linear, center-fed antenna [19]. An increase of the minor axis blue-shifts

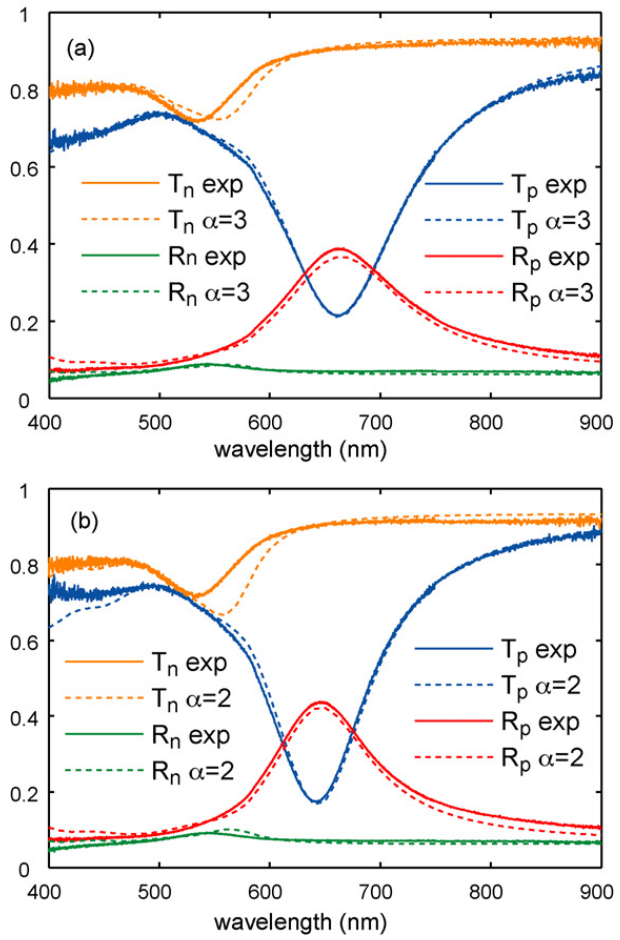


Fig. 4. The transmittance ($T$) and reflectance ($R$) spectra of samples A and B for both principal polarization (p) and secondary polarization (n). The experimental spectra (exp) are compared to the simulated spectra using the Drude–Lorentz model with loss factor $\alpha = 3$ for sample A (a) and $\alpha = 2$ for sample B (b).

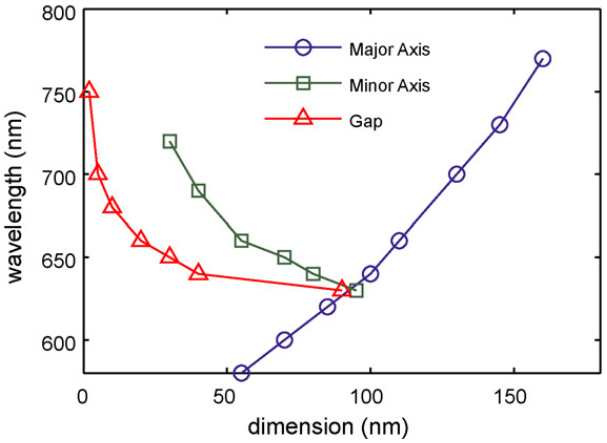


Fig. 5. The resonance wavelengths as functions of major axis, minor axis, and gap.

the resonance. When the minor axis is long and close to the major axis, the particles are similar to nanodiscs so we have the resonance of paired nanodiscs; when the minor axis is small, the particles are like nanorods so we have the resonance of paired nanorods. The resonant wavelength is very sensitive to the gap when the gap is small but does not shift much when the gap is large. When the gap is small, the coupling between the pair is strong and therefore sensitive to the gap; when the gap is large, the coupling is weak and we basically observe a single particle resonance which does not strongly depend on the size of the gap. This exponential-like resonance shift caused by the gap is similar to the results obtained for gold nanodisc pairs using the DDA method and can be explained by the coupling of surface plasmons between the gold particle pairs [26,28].

Many applications of nanoantennas, such as NSOM and surface-enhanced Raman scattering (SERS), rely on the nanoantenna near-field characteristics, especially in the "hot spot," i.e. an area with high enhancement of the local field (the amplitude of the local electric field normalized by the incident electric field). Such a hot spot generated by sample A is prominent in the electric field enhancement map, which is plotted at 20 nm above the substrate for the principal polarization at a wavelength of 680 nm (Fig. 6(a)). The electric field enhancement inside the gap is more than 10, but the hot spot is confined by the gap. Outside of the gap the electric field is also enhanced in the area close to the gold particle, but to a lesser extent. The strength of the resonance is a function of wavelength. The electric field enhancement at the center of the gap is plotted versus incident wavelength in Fig. 6(b). The near-field resonance, where the field enhancement is the highest, is at 680, 20 nm red-shifted compared to the far-field resonance at 660 nm.

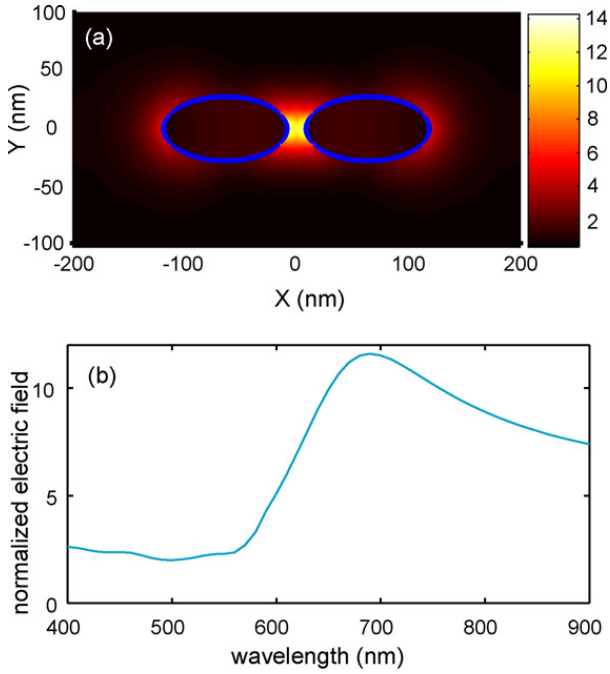


Fig. 6. (a) The normalized electric field map of a unit cell in sample A at 20 nm above the substrate at a wavelength of 680 nm. The particle outlines are shown for reference (blue ellipses). (b) The normalized electric field at the gap center 20 nm above the substrate as a function of wavelength.

This red-shift is consistent with other authors' observations [18].

The field enhancement also depends on the antenna geometry. The dimensions of sample A are varied in simulations as before, and the on-resonance electric field enhancement at the center of the gap 20 nm above the substrate for the principal polarization is plotted as a function of the major axis, the minor axis, and the gap (Fig. 7). From Fig. 7 we see that the local field strength

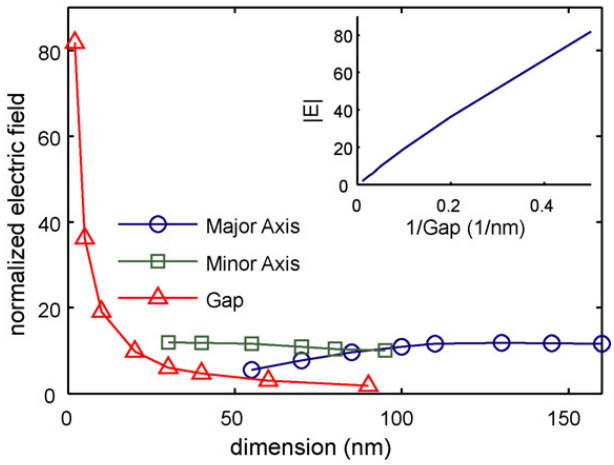


Fig. 7. The normalized electric field strength as a function of major axis, minor axis, and gap. The inset shows that the electric field strength is inversely proportional to the gap size.

increases with major axis length but saturates after a certain value, while it is nearly independent of minor axis length. The field enhancement is found to be roughly inversely proportional to the gap size (Fig. 7 inset), therefore shrinking the gap is the most effective way to increase the local field. However, this technique is most useful for small gaps since it is only for small gaps that the coupling between the pair begins to emerge.

## 3. Conclusions

We have demonstrated that FEM simulations can accurately model the far-field spectra of optical nanoantenna arrays in the visible range if material property modification for fabricated nanostructures as compared to bulk data is taken into account. For the optical nanoantenna arrays composed of paired gold elliptical cylinders, the resonant wavelength red-shifts with an increase of the nanoparticle major axis and blue-shifts with an increase of the minor axis. Decreasing the gap also red-shifts the resonance, and the shift has an exponential-like relation with the gap size. The near-field hot spot is confined inside the gap. Changing the major axis and minor axis has only limited effects on the field enhancement. The field enhancement at the center of the gap of the nanoantenna pairs is inversely proportional to the gap size, so decreasing the gap size is an effective way to achieve large field enhancement.

## Acknowledgements

This work is supported in part by ARO-STTR award W911NF-07-C-0008. A. B. acknowledges support from the Danish Research Agency (NABIIT programme committee, grant 2106-05-0033). The authors wish to thank Samuel Gresillon at CNRS and Universite Pierre et Marie Curie Paris 6 for many fruitful discussions and Mark Stockman at Georgia State University for discussions on the field-gap relation.

## References

[1] P. Muhlschlegel, H.J. Eisler, O.J.F. Martin, B. Hecht, D.W. Pohl, Resonant optical antennas, Science 308 (2005) 1607–1609.
[2] J.P. Kottmann, O.J.F. Martin, Plasmon resonant coupling in metallic nanowires, Opt. Express 8 (2001) 655–663.
[3] M. Moskovits, Surface-enhanced Raman spectroscopy: a brief retrospective, J. Raman Spectrosc. 36 (2005) 485–496.
[4] E.Y. Poliakov, V.M. Shalaev, V.A. Markel, R. Botet, Enhanced Raman scattering from self-affine thin films, Opt. Lett. 21 (1996) 1628–1630.
[5] A.M. Dykhne, A.K. Sarychev, V.M. Shalaev, Resonant transmittance through metal films with fabricated and light-induced modulation, Phys. Rev. B 67 (2003) 195402.
[6] V.M. Shalaev, R. Botet, A.V. Butenko, Localization of collective dipole excitations on fractals, Phys. Rev. B 48 (1993) 6662–6664.
[7] A.V. Butenko, V.M. Shalaev, M.I. Stockman, Fractals—giant impurity nonlinearities in optics of fractal clusters, Z. Phys. D Atom Mol. Clust. 10 (1988) 81–92.
[8] S.A. Maier, M.L. Brongersma, P.G. Kik, S. Meltzer, A.A.G. Requicha, H.A. Atwater, Plasmonics—a route to nanoscale optical devices, Adv. Mater. 13 (2001) 1501–1505.
[9] W. Rechberger, A. Hohenau, A. Leitner, J.R. Krenn, B. Lamprecht, F.R. Aussenegg, Optical properties of two interacting gold nanoparticles, Opt. Commun. 220 (2003) 137–141.
[10] J.N. Farahani, D.W. Pohl, H.-J. Eisler, B. Hecht, Single quantum dot coupled to a scanning optical antenna: a tunable superemitter, Phys. Rev. Lett. 95 (2005) 017402.
[11] J.N. Farahani, H.-J. Eisler, D.W. Pohl, M. Pavius, P. Flückiger, P. Gasser, B. Hecht, Bow-tie optical antenna probes for single-emitter scanning near-field optical microscopy, Nanotechnology 18 (2007) 125506.
[12] B. Hecht, P. Mühlschlegel, J.N. Farahani, H.-J. Eisler, D.W. Pohl, O.J.F. Martin, P. Biagioni, Prospects of resonant optical antennas for nano-analysis, Chimia 60 (2006) 765–769.
[13] E. Cubukcu, E.A. Kort, K.B. Crozier, F. Capasso, Plasmonic laser antenna, Appl. Phys. Lett. 89 (2006) 093120.
[14] A. Sundaramurthy, P.J. Schuck, N.R. Conley, D.P. Fromm, G.S. Kino, W.E. Moerner, Toward nanometer-scale optical photolithography: utilizing the near-field of bowtie optical nanoantennas, Nano Lett. 6 (2006) 355–360.
[15] T. Søndergaard, S.I. Bozhevolnyi, Metal nano-strip optical resonators, Opt. Express 15 (2007) 4198–4204.
[16] T. Søndergaard, S. Bozhevolnyi, Slow-plasmon resonant nanostructures: scattering and field enhancements, Phys. Rev. B 75 (2007) 073402.
[17] S.I. Bozhevolnyi, T. Søndergaard, General properties of slow-plasmon resonant nanostructures: nano-antennas and resonators, Opt. Express 15 (2007) 10869–10877.
[18] J. Aizpurua, G.W. Bryant, L.J. Richter, F.J. García de Abajo, Optical properties of coupled metallic nanorods for field-enhanced spectroscopy, Phys. Rev. B 71 (2005) 235420.
[19] K.B. Crozier, A. Sundaramurthy, G.S. Kino, C.F. Quate, Optical antennas: resonators for local field enhancement, J. Appl. Phys. 94 (2003) 4632–4642.
[20] D.P. Fromm, A. Sundaramurthy, P.J. Schuck, G. Kino, W.E. Moerner, Gap-dependent optical coupling of single "bowtie" nanoantennas resonant in the visible, Nano Lett. 4 (2004) 957–961.
[21] D.P. Fromm, A. Sundaramurthy, A. Kinkhabwala, P.J. Schuck, G.S. Kino, W.E. Moerner, Exploring the chemical enhancement for surface-enhanced Raman scattering with Au bowtie nanoantennas, J. Chem. Phys. 124 (2006) 061101.
[22] E. Hao, G.C. Schatz, Electromagnetic fields around silver nanoparticles and dimers, J. Chem. Phys. 120 (2004) 357–366.
[23] P.J. Schuck, D.P. Fromm, A. Sundaramurthy, G.S. Kino, W.E. Moerner, Improving the mismatch between light and nanoscale objects with gold bowtie nanoantennas, Phys. Rev. Lett. 94 (2005) 017402.
[24] A. Sundaramurthy, K.B. Crozier, G.S. Kino, D.P. Fromm, P.J. Schuck, W.E. Moerner, Field enhancement and gap-dependent resonance in a system of two opposing tip-to-tip Au nanotriangles, Phys. Rev. B 72 (2005) 165409.
[25] S. Enoch, R. Quidant, G. Badenes, Optical sensing based on plasmon coupling in nanoparticle arrays, Opt. Express 12 (2004) 3422–3427.

[26] P.K. Jain, W. Huang, M.A. El-Sayed, On the universal scaling behavior of the distance decay of plasmon coupling in metal nanoparticle pairs: a plasmon ruler equation, Nano Lett. 7 (2007) 2080–2088.
[27] I. Romero, J. Aizpurua, G.W. Bryant, F.J. García de Abajo, Plasmons in nearly touching metallic nanoparticles: singular response in the limit of touching dimers, Opt. Express 14 (2006) 9988–9999.
[28] K.-H. Su, Q.-H. Wei, X. Zhang, J.J. Mock, D.R. Smith, S. Schultz, Interparticle coupling effects on plasmon resonances of nanogold particles, Nano Lett. 3 (2003) 1087–1090.
[29] H. Wang, D.W. Brandl, P. Nordlander, N.J. Halas, Plasmonic nanostructures: artificial molecules, Acc. Chem. Res. 40 (2007) 53–62.
[30] J. Li, A. Salandrino, N. Engheta, Shaping light beams in the nanometer scale: a Yagi-Uda nanoantenna in the optical domain, Phys. Rev. B 76 (2007) 245403.
[31] R.M. Bakker, A. Boltasseva, Z. Liu, R.H. Pedersen, S. Gresillon, A.V. Kildishev, V.P. Drachev, V.M. Shalaev, Near-field excitation of nanoantenna resonance, Opt. Express 15 (2007) 13682–13688.
[32] P.B. Johnson, R.W. Christy, Optical constants of the noble metals, Phys. Rev. B 6 (1972) 4370–4379.
[33] S. Link, M.A. El-Sayed, Spectral properties and relaxation dynamics of surface plasmon electronic oscillations in gold and silver nanodots and nanorods, J. Phys. Chem. B 103 (1999) 8410–8426.
[34] S. Zhang, W. Fan, N.C. Panoiu, K.J. Malloy, R.M. Osgood, S.R.J. Brueck, Experimental demonstration of near-infrared negative-index metamaterials, Phys. Rev. Lett. 95 (2005) 137404.
[35] G. Dolling, M. Wegener, C.M. Soukoulis, S. Linden, Negative-index metamaterial at 780 nm wavelength, Opt. Lett. 32 (2007) 53–55.
[36] H.-K. Yuan, U.K. Chettiar, W. Cai, A.V. Kildishev, A. Boltasseva, V.P. Drachev, V.M. Shalaev, A negative permeability material at red light, Opt. Express 15 (2007) 1076–1083.
[37] A.V. Kildishev, U.K. Chettiar, H.-K. Yuan, W. Cai, V.M. Shalaev, Optimizing optical negative index materials: feedback from fabrication, in: 23rd Annual Review of Progress in Applied Computational Electromagnetics, Verona, Italy, 2007, pp. 943–948.
[38] V.P. Drachev, U.K. Chettiar, H. Yuan, W. Cai, A.V. Kildishev, V.M. Shalaev, Size Effects in Plasmonic Metamaterials for the Visible Range, SPIE Optics Photonics, San Diego, CA, USA, 2007, pp. 6642–6632.
[39] V.P. Drachev, U.K. Chettiar, A.V. Kildishev, H.-K. Yuan, W. Cai, V.M. Shalaev, The Ag dielectric function in plasmonic metamaterials, Opt. Express 16 (2008) 1186–1195.